

Feasibility studies for triple Higgs boson production in the $4b2\tau$ final state at the FCC-hh

Thomas Dingley^{1*}, James Frost^{1,2*} and Holly Pacey^{1*}

¹Department of Physics, University of Oxford, Keble Road, Oxford, United Kingdom.

²Particle Physics Department, Rutherford Appleton Laboratory, Didcot, United Kingdom.

*Corresponding author(s). E-mail(s): thomas.dingley@physics.ox.ac.uk; james.frost@cern.ch; holly.ann.pacey@cern.ch;

Abstract

A feasibility study of triple Higgs boson production at the Future Circular Collider proton–proton stage, FCC-hh, at a centre-of-mass energy $\sqrt{s} = 84$ TeV has been performed in the $4b2\tau$ final state. SM-like HHH signals are studied. Both the mixed leptonic-hadronic ($\tau_{\text{lep}}\tau_{\text{had}}$) and fully hadronic ($\tau_{\text{had}}\tau_{\text{had}}$) decay modes of the τ -lepton pair are considered in orthogonal channels and combined. For each channel, a neural network classifier is trained to improve experimental sensitivity by discriminating between the HHH signals and Standard Model backgrounds, utilising kinematic features of the events’ reconstructed objects and Higgs boson candidates. Considering a conservative jet flavour identification uncertainty (uncertainty Scenario I), a 95% upper cross-section limit of $3 \times \sigma_{HHH}^{SM}$ is expected, with the $\tau_{\text{had}}\tau_{\text{had}}$ channel leading in sensitivity. The sensitivity of this final state to constrain the tri-linear and quartic Higgs self-couplings is evaluated for several uncertainty scenarios. Assuming the SM value of the trilinear self-coupling, a constraint is derived on the quartic self-coupling of between -5.6 and 21 times the SM value at 68% CL. In combination with other triple-Higgs final states, this result demonstrates the potential of the FCC-hh to constrain the quartic Higgs self-coupling.

1 Introduction

Since the discovery of the Higgs boson by the ATLAS and CMS experiments in 2012, a rich and wide-ranging suite of measurements probing its properties have been performed, including its mass, width and its couplings to fermions and gauge-bosons. Furthermore, measurements probing the electroweak symmetry breaking mechanism (EWSB) via the shape of the Higgs-potential are a crucial component of the LHC physics programme.

The Higgs-potential may be parametrised as

$$V(H) = \frac{1}{2}m_H^2 H^2 + \kappa_3 \lambda v H^3 + \frac{\kappa_4}{4} \lambda H^4 \quad (1)$$

where m_H is the mass of the SM Higgs boson, v is the vacuum expectation value, $\lambda = \frac{m_H^2}{2v^2}$ and κ_3 and κ_4 are the ratios of the tri-linear and quartic Higgs self-couplings to their SM predictions ($\kappa_i = \lambda_i/\lambda_i^{SM}$), such that $\kappa_3 = \kappa_4 = 1$ in the SM [1]. To constrain κ_3 directly, di-Higgs production (HH) is needed, however direct constraint of κ_4 requires the study of triple-Higgs production (HHH). Complementary κ_4 sensitivity may result from indirect methods, utilising EW-loop level corrections to HH production [2, 3].

Production of HHH at hadron colliders is an exceptionally rare process in the SM and upon completion of 3 ab⁻¹ of $\sqrt{s} = 14$ TeV data-taking at HL-LHC, where the Next-to-Next-to-Leading-Order (NNLO) HHH production cross-section is $\sigma_{HHH}^{SM} = 0.103$ fb, the expected yield of HHH events is only $\mathcal{O}(10^2)$. Compared to the HH yield of $\mathcal{O}(10^5)$, the challenge of constraining κ_4 relative to κ_3 is clear. Measurements have been performed by the ATLAS [4] and CMS [5] collaborations in the $6b$ and $4b2\gamma$ final states respectively, yielding expectedly weak constraints on the quartic self-coupling. Upon completion of the high-luminosity LHC runs, ATLAS and CMS are expected to constrain $\kappa_3 \in [0.7, 1.3]$ and $\kappa_4 \in [-84, 96]$ for $\kappa_3 = 1$ at 95% confidence level (CL) in the $6b$ -channel [6]. Only modest improvements of this limit are expected through improved reconstruction techniques and combination with additional channels. Notably, it is not foreseen that these limits will appreciably probe the space not excluded by perturbative unitarity constraints [7].

SM-like HHH production at hadron colliders predominantly arises via gluon-gluon fusion with top-quark loops; the four leading diagrams, alongside the associated dependency on the coupling-modifiers, are shown in Figure 1. With the significant increase in collision energy at the proposed FCC-hh, the cross-section for gluon-gluon fusion processes exponentially increases, and the σ_{HHH}^{SM} NNLO prediction at $\sqrt{s} = 84$ (100) TeV is 3.56 (5.56) fb [8]. At the baseline $\sqrt{s} = 84$ TeV considered in this analysis, the production cross-section is thus 53.98 \times larger than the HL-LHC prediction, and the expected yield of SM HHH events is $\mathcal{O}(10^5)$. Given the higher-statistics, one can expect otherwise statistically limited, but experimentally cleaner signatures such as $4b2\gamma$ and $4b2\tau$ channels to prove powerful compared with the previously probed $6b$ channel. A breakdown of channel statistics is provided in Table 1.

This note documents an analysis of the $4b2\tau$ channel, with fewer irreducible backgrounds and a more readily reconstructed final state than $6b$. Feasibility studies are

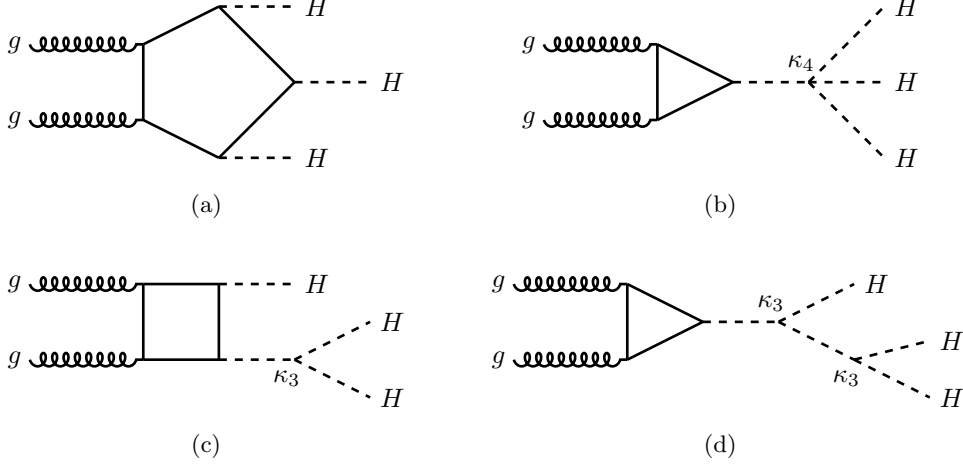


Fig. 1: Feynman diagrams for leading-order [QCD] $gg \rightarrow HHH$ production via a quark loop. The dominant production mechanism is shown in (a), whilst sub-leading diagrams (b), (c) and (d) are sensitive to κ_4 , κ_3 and κ_3^2 respectively, as indicated by labels.

Table 1: Expected number of HHH events in various Higgs boson decay channels at $\sqrt{s} = 84$ TeV and $\mathcal{L} = 30$ ab^{-1} , assuming SM Higgs boson branching ratios (BRs) from Ref. [9].

Final state	BR expression	Expected events (30 ab^{-1})
$6b$	$(0.58)^3$	20,819
$4b2\tau$	$3 \times (0.58)^2 \times 0.063$	6,791
$4\tau2b$	$3 \times (0.063)^2 \times 0.58$	761
$4b2\gamma$	$3 \times (0.58)^2 \times 0.0023$	247
$2\tau2\gamma2b$	$6 \times 0.58 \times 0.063 \times 0.0023$	93
6τ	$(0.063)^3$	27
$4b2W$	$3 \times (0.58)^2 \times 0.215$	23,200
$2b4W$	$3 \times 0.58 \times (0.215)^2$	8,571
$6W$	$(0.215)^3$	1,055

performed to establish the expected sensitivity to SM HHH production cross-section, σ_{HHH}^{SM} , at the FCC-hh. Furthermore the expected sensitivity of using HHH production to constrain SM-like scenarios with κ_3 and κ_4 modified from their expected SM values, is investigated. The note is structured as follows. First, a summary of the Monte Carlo (MC) simulated events used is given in Section 2. Section 3 explains how events are reconstructed and Section 4 describes the event selection process used to obtain sensitivity. The statistical analysis procedure is detailed in Section 5 followed by a description of the systematic uncertainties considered in Section 6. The results are presented in Section 7, with final conclusions drawn in Section 8.

2 Monte Carlo simulations

The baseline detector concept used for the FCC-hh physics studies is described in Refs. [10, 11], wherein Scenario-II is used. All samples are simulated using the DELPHES framework [12], with the parametrisation documented in Ref. [13]. The samples are then further processed for analysis using the **Key4hep** framework [14]. With the large centre-of-mass energy and instantaneous luminosity, the pileup profile is significant, reaching $\mathcal{O}(1000)$ additional interactions along the beamline. Despite this, pile-up is not considered in the analysis, since studies into the FCC-hh pile-up mitigation performance are on-going and techniques are foreseen to significantly improve with the experience gained during the HL-LHC - operating nominally around an average pile-up of $\mathcal{O}(200)$. Including the harsh pile-up profile without such advanced techniques deployed therefore would be overly conservative.

MC simulated samples are used for all signal and background processes in this analysis. All processes are generated at leading order with MADGRAPH 5 [15], partons showered and decayed with PYTHIA 8.311 [16], and smeared with the DELPHES fast simulation of the FCC-hh Scenario II detector concept. The $H \rightarrow b\bar{b}$ branching fraction is set as 0.582, and its total width 4.088 MeV, corresponding to the SM values for a Higgs boson mass of 125 GeV [9]. In line with other FCC-hh feasibility studies, the **MMHT2015qed_nlo** PDF set is used.

Signal samples for HHH production are generated assuming the SM values of $(\kappa_3, \kappa_4) = (1, 1)$, including all diagrams shown in Figure 1 with full interference. Sample re-weighting is used to obtain events at different (κ_3, κ_4) values. This is implemented using the MADGRAPH 5 re-weighting tool [17], following a similar procedure to that outlined in Ref. [18]. Variations in the cross-section across the (κ_3, κ_4) plane considered are shown in Figure 2. The values of (κ_3, κ_4) determine the interference between the diagrams, which impact the resultant event kinematics.

SM background processes generated include the dominant $t\bar{t}$ processes with additional b -jets ($t\bar{t} + b\bar{b}$), and sub-dominant processes including $t\bar{t}H$, $t\bar{t}Z$, ZZZ and $t\bar{t}t\bar{t}$. Other SM background processes such as HH , $Z + \text{jets}$ and diboson are expected to give small contributions and are left for future studies. Irreducible non-resonant backgrounds such as QCD are not included but expected to be small or reducible via a continuum background subtraction approach.

3 Event reconstruction

DELPHES provides a parametrised detector response, with resolution functions and efficiency factors for particle reconstruction and identification. Physics objects such as tracks and calorimeter clusters are generated, along with analysis objects such as leptons, jets, jet flavour assignments and missing transverse momentum E_T^{miss} . Hadronic jet reconstruction is performed using a particle flow method that integrates track and calorimeter data to yield particle flow candidates, which are also used for leptonic isolation and E_T^{miss} determination.

Hadronic jets are reconstructed using the anti- k_T clustering algorithm [19] with a radius parameter of 0.4, from particle-flow objects. They are required to have a $p_T > 25$ GeV and $|\eta| < 4$.

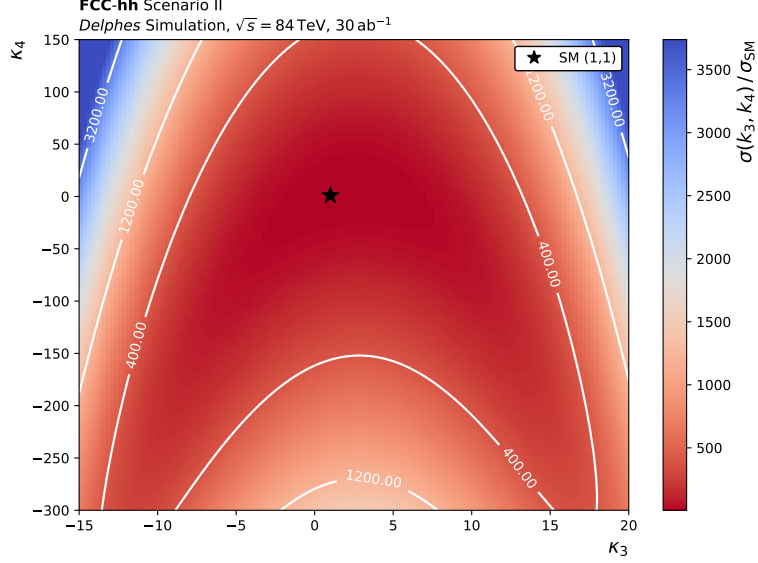


Fig. 2: The relative HHH production cross-sections at $\sqrt{s} = 84$ TeV as a function of the SM cross-section σ_{HHH}^{SM} across the (κ_3, κ_4) plane.

Truth-particles are associated to reconstructed jets with a matching radius of 0.3. The jets, with the corresponding flavour association, are passed through the respective identification efficiency map, parametrised as a function of jet p_T and η . Jets originating from B -hadrons are identified from the total visible four-momentum of the jet candidates using the Medium identification working point defined in Ref. [13]. Hadronically decaying τ candidates (τ_{had}) are reconstructed from the total visible four-momentum of the jet candidates using the Medium identification working point defined in Ref. [13]. They are required to have a $p_T > 25$ GeV and $|\eta| < 4$.

For both b -jet and τ_{had} identification algorithms, (mis-)tagging efficiencies rely on a parametrisation in jet p_T and η . These efficiencies are inspired by current transformer-based tagging algorithms employed at the CMS experiment [20, 21], and are fully described in Ref. [13]. The assumed b -jet tagging efficiency ϵ_b ranges from 75 – 85%, and the light (charm) jet mis-tag rates range from 0.6 – 1.5% (10 – 20)%, across p_T and η . The assumed τ_{had} tagging efficiency ϵ_τ is 80 – 88% depending on the p_T of the τ_{had} candidate, the hadronic jet mis-tag rates ϵ_j are 1 – 2% depending upon the p_T of the jet. An overlap removal procedure is applied to the b -jet and τ_{had} candidates to avoid double-counting.

Electron and muon candidates, defined by DELPHES, are required to have a $p_T > 20$ GeV and $|\eta| < 4$. Electron and muon reconstruction and identification efficiencies are parametrised as functions of p_T and η . For each given electron (muon) candidate, all

particle flow objects within $\Delta R < 0.3$ are used to define:

$$I(l) = \frac{\sum_{i[\Delta R < 0.3]} p_T^i}{p_T(l)} \quad (2)$$

To remove the contribution of both non-prompt leptons and leptons originating from a B-hadron decay, the following isolation criterion is applied. Electron and muon candidates are considered isolated if $I < 0.2$. The four-momenta of b -jets are corrected through the inclusion of non-isolated muons within $\Delta R < 0.4$ of the jet axis, which improves the mean reconstructed Higgs boson mass and (slightly) its resolution.

The detector signature for stable invisible particles produced at FCC-hh is missing transverse momentum. The two-dimensional missing transverse momentum vector \vec{p}_T^{miss} is computed as the negative vector sum of the p_T of all the reconstructed particle flow objects in an event. The magnitude of this vector, E_T^{miss} , is the missing transverse momentum value used in the analysis. Associated to the E_T^{miss} is the E_T^{miss} significance, estimated as $E_T^{\text{miss}}/\sqrt{H_T}$, where H_T is defined by the scalar sum of the p_T of the particle flow objects in the event.

4 Event selection

Two orthogonal analysis channels are considered which target different decay modes of the pair of τ -leptons originating from one of the Higgs boson decays: $\tau_{\text{lep}}\tau_{\text{had}}$, targeting the case where one *tau* decays hadronically and the other leptonically (to either an electron or muon) and $\tau_{\text{had}}\tau_{\text{had}}$, targeting the case where both decay hadronically. In each channel, a set of Preselection requirements are applied to all events for use in the analysis. Subsequently, in each channel a Neural Network (NN) classifier is trained to discriminate between the HHH signal and SM backgrounds, and a requirement is placed on the NN output score to define two single-bin search regions (SR- $\tau_{\text{lep}}\tau_{\text{had}}$ and SR- $\tau_{\text{had}}\tau_{\text{had}}$). To produce the final results the SR- $\tau_{\text{lep}}\tau_{\text{had}}$ and SR- $\tau_{\text{had}}\tau_{\text{had}}$ regions are fit simultaneously. A summary of the event selection is given in Table 2.

4.1 Preselection

Events are required to contain exactly four b -tagged jets and two τ -lepton candidates, with no additional charged leptons (e or μ) present beyond those from the corresponding τ -lepton decays. For both channels, the B -hadron jets from Higgs boson decays are targeted by slightly raised selections on their transverse momenta, with the leading three b -jets required to be greater than 40, 35 and 30 GeV, respectively.

Two oppositely-charged (OS) hadronic- τ candidates with the medium working point are required for the $\tau_{\text{had}}\tau_{\text{had}}$ channel. For the $\tau_{\text{lep}}\tau_{\text{had}}$ channel, oppositely charged pairs formed from one electron or muon, and one hadronic τ candidate, are required.¹

¹The p_T distribution of the charged leptons from the τ -lepton decay is relatively soft, thus there would be an efficiency gain were it possible to lower the $p_T > 20$ GeV requirement in the FCC-hh environment.

Table 2: Summary of the event Preselection for the $\tau_{\text{had}}\tau_{\text{had}}$ and $\tau_{\text{lep}}\tau_{\text{had}}$ channels, and definitions of SR- $\tau_{\text{lep}}\tau_{\text{had}}$ and SR- $\tau_{\text{had}}\tau_{\text{had}}$.

Variable	$\tau_{\text{lep}}\tau_{\text{had}}$	$\tau_{\text{had}}\tau_{\text{had}}$
Preselection		
$n(b)$		$==4$
$p_{\text{T}}(b_1)$ [GeV]		> 40
$p_{\text{T}}(b_2)$ [GeV]		> 35
$p_{\text{T}}(b_3)$ [GeV]		> 30
$p_{\text{T}}(b_4)$ [GeV]		> 25
$n(\tau_{\text{had}})$	$==1$	$==2$
$n(l = e/\mu)$	$==1$	$==0$
τ charges	$OS(\tau_{\text{had}}, l)$	$OS(\tau_{\text{had}}, \tau_{\text{had}})$
$p_{\text{T}}(\tau_{\text{had}1})$ [GeV]		> 25
$p_{\text{T}}(\tau_{\text{had}2})$ [GeV]	-	> 25
$p_{\text{T}}(l)$ [GeV]	> 20	-
SR- $\tau_{\text{lep}}\tau_{\text{had}}$		SR- $\tau_{\text{had}}\tau_{\text{had}}$
Preselection	Pass	
NN Score	$NN_{\text{lephad}} > 0.9875$	$NN_{\text{hadhad}} > 0.9875$

4.2 Higgs boson candidate reconstruction

The kinematic properties of the Higgs boson candidates are helpful in discriminating between the signal and SM backgrounds. To reconstruct the four-momentum of the Higgs boson that decays into a pair of τ -leptons, the four-momentum of the $\tau\tau$ system is used. The Higgs boson mass is defined by the visible part of the reconstructed $\tau\tau$ invariant mass ($m_{\tau\tau}^{\text{vis-OS}}$). The distributions of the reconstructed Higgs boson mass for each of the HHH signal and SM background processes are shown in Figure 3, in the $\tau_{\text{lep}}\tau_{\text{had}}$ and $\tau_{\text{had}}\tau_{\text{had}}$ channels, showing the expected behaviour that the signal mass peaks below 125 GeV due to the missing invisible component.²

To reconstruct the two Higgs boson candidates that each decay into pairs of b -jets, a pairing algorithm is applied to events passing the Preselection to decide which of the four b -jets originate from which Higgs boson decay. The optimal pairing algorithm found is defined by minimising the greatest angular separation between the Higgs boson candidates decay products (jets i, j, k, l). This can be expressed as:

$$\min(\Delta R_{\text{max}}(b, b)) = \min_{i,j,k,l} (\max(\Delta R(i, j), \Delta R(k, l))). \quad (3)$$

The two Higgs boson candidates are then numbered in descending p_{T} .

The distributions of the higher p_{T} reconstructed Higgs boson mass for each of the HHH signal and SM background processes are shown in Figure 4. This shows the successful identification of a resonance around the Higgs boson mass for the HHH signal and $t\bar{t}H$ background which contain a real Higgs boson. It also shows an expected

²It is expected that analysis sensitivity can be improved by using the Missing-Mass-Calculator [22] to estimate the full $\tau\tau$ invariant mass including the invisible component. This is planned for inclusion in a future iteration of the analysis.

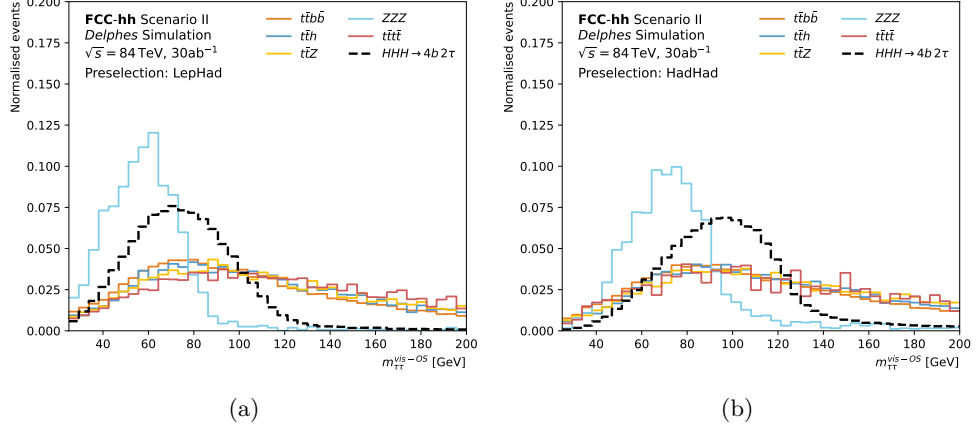


Fig. 3: Distributions of the $H \rightarrow \tau\tau$ candidate mass ($m_{\tau\tau}^{\text{vis-OS}}$) for the HHH signal and stacked SM backgrounds. The (a) $\tau_{\text{lep}}\tau_{\text{had}}$ and (b) $\tau_{\text{had}}\tau_{\text{had}}$ channels are shown with the Preselection applied. Histograms are normalised to unit area.

peak at the Z -boson mass for the $t\bar{t}Z$ and ZZZ processes, well-separated from the signal distribution, and broad distributions for the non-resonant $t\bar{t}$ and $t\bar{t}t\bar{t}$ processes. The overall signal-background discrimination provided by the reconstructed masses of the Higgs boson candidates decaying into b -jets is further illustrated in the stacked histograms in Figure 5.

4.3 Machine Learning

Although the Preselection is effective at eliminating a large portion of the SM background, the HHH signature is of exceptionally low cross-section and hence benefits from the use of machine learning classifiers to enhance sensitivity. For each of the $\tau_{\text{lep}}\tau_{\text{had}}$ and $\tau_{\text{had}}\tau_{\text{had}}$ channels, a NN classifier ($\text{NN}_{\text{lephad}}$, $\text{NN}_{\text{hadhad}}$) is trained to discriminate between the HHH signal and SM backgrounds, and a cut is placed on the resulting NN output score to define the search region in that channel.

Input features to the NNs are chosen from kinematic variables related to the kinematics of the b -jets, τ -leptons, reconstructed Higgs boson candidates, $E_{\text{T}}^{\text{miss}}$ and event-wide variables. An example important variable for each network is shown in Figure 6. In particular, there is significant discriminating power in the reconstructed Higgs boson candidate masses, as the SM backgrounds lack the triply-resonant structure of the HHH signal. With variations in κ_3 and κ_4 manifesting in varied event-wide kinematic distributions, care is needed when choosing the classifier's input feature set to avoid performance loss away from the SM signal used for training. An example of such variations is shown in Figure 7, where strong shape variations across κ_3 and κ_4 are observed. Resonant features targeting specific Higgs boson kinematics are invariant across the (κ_3, κ_4) plane, and thus prove beneficial in rejecting background whilst remaining robust across the targeted parameter space.

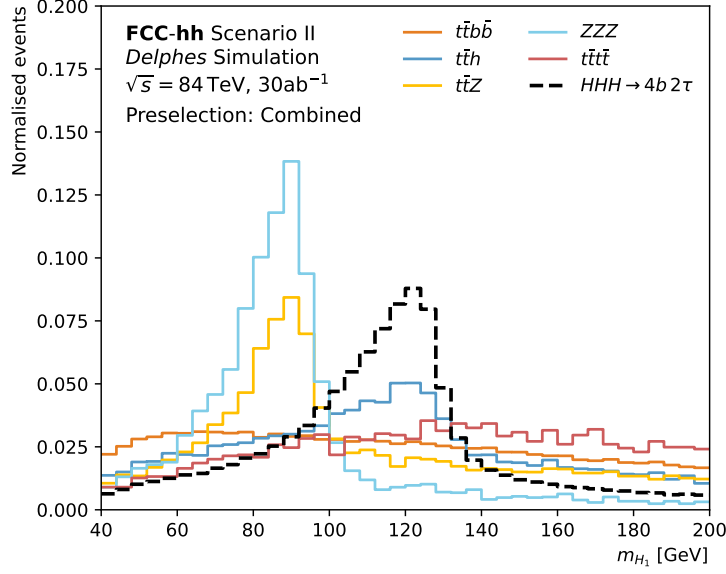


Fig. 4: Distributions of the leading $h \rightarrow b\bar{b}$ candidate mass (m_{H_1}) for the HHH signal and SM backgrounds. The $\tau_{\text{had}}\tau_{\text{had}}$ and $\tau_{\text{lep}}\tau_{\text{had}}$ channels combined are shown with the Preselection and pairing algorithm applied. Histograms are normalised to unit area.

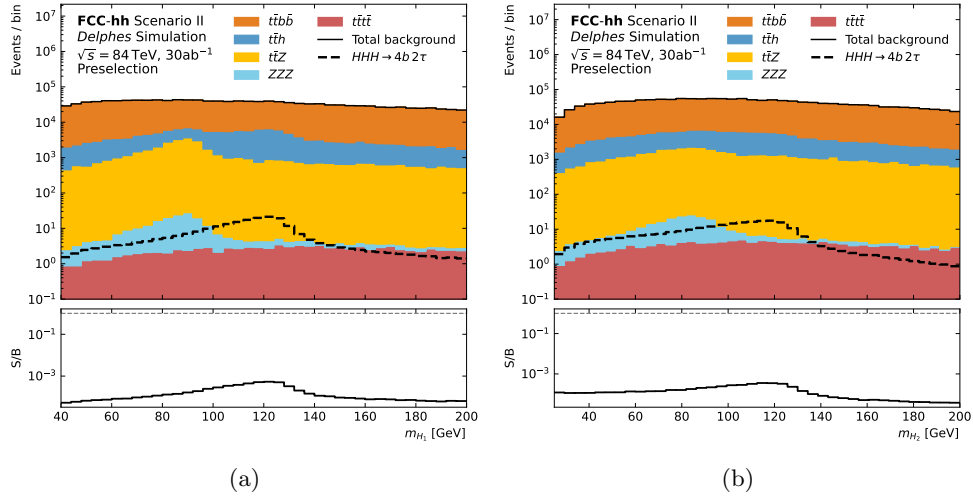


Fig. 5: Distributions of the (a) leading and (b) sub-leading $H \rightarrow b\bar{b}$ candidate masses for the HHH signal and stacked SM backgrounds. The $\tau_{\text{had}}\tau_{\text{had}}$ and $\tau_{\text{lep}}\tau_{\text{had}}$ channels combined are shown with the Preselection and pairing algorithm applied. The lower panel shows the signal to background ratio.

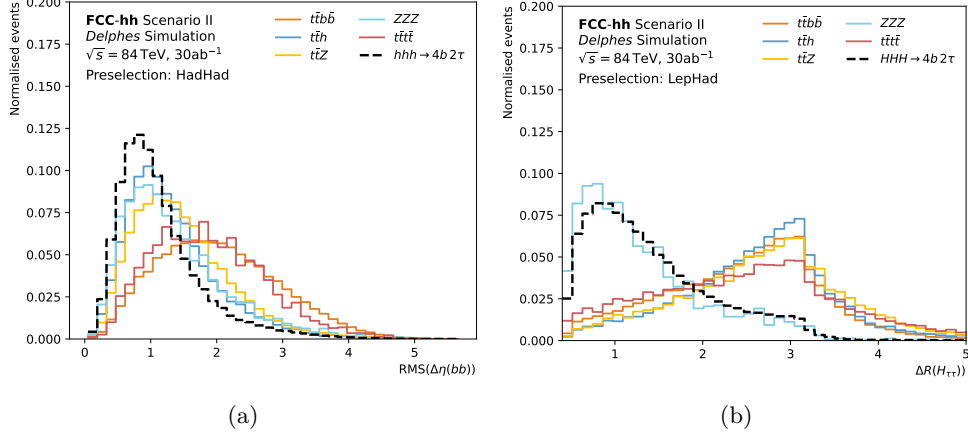


Fig. 6: Example distributions of kinematic variables important to each NN for the HHH signal and each SM backgrounds: (a) the root-mean-square of the η difference between all possible pairs of b -jets in the $\tau_{\text{had}}\tau_{\text{had}}$ channel and (b) the ΔR between the τ_{had} and lepton in the $\tau_{\text{lep}}\tau_{\text{had}}$ channel. The Preselection is applied. Histograms are normalised to unit area.

The NNs are implemented using Scikit-Learn [23]. The **Optuna** framework [24] is used to optimise the hyper-parameters in each network. For both NNs, an architecture with two hidden layers is chosen, with 256 hidden nodes in the first layer and 128 in the second. Rectified linear unit (ReLU) activation is used. A standard Binary Cross-Entropy loss function is used. For $\text{NN}_{\text{lep}}\tau_{\text{had}}$ ($\text{NN}_{\text{had}}\tau_{\text{had}}$) a batch size of 512 (256) is used, a learning rate of 0.01104 (0.002695) and an early-stopping patience of 15 (13) epochs.

The networks are trained on SM HHH signal and SM background events passing the Preselection, amounting to a total training dataset of size 4×10^5 events. Equal sets of signal and background events are used for training, with the composition of the background set following that of the preselection. To avoid overtraining and benefit from the full set of available simulated samples, orthogonal training and testing/validation datasets are used. These are defined through a k -fold splitting procedure with $k = 2$ [25].

The score distributions are shown in Figure 8, illustrating the HHH signals successfully peaking at the ‘signal-like’ score of 1 and the SM backgrounds peaking at the ‘background-like’ score of 0. To define $\text{SR-}\tau_{\text{lep}}\tau_{\text{had}}$ ($\text{SR-}\tau_{\text{had}}\tau_{\text{had}}$), the $\text{NN}_{\text{lep}}\tau_{\text{had}}$ ($\text{NN}_{\text{had}}\tau_{\text{had}}$) score is required to be greater than 0.9875.

5 Statistical Analysis

A combined likelihood is constructed for the two independent channels and the corresponding profile likelihood ratio is maximised. The common fitted parameter of interest, μ , is the signal strength of a given (κ_3, κ_4) prediction, defined as the ratio of

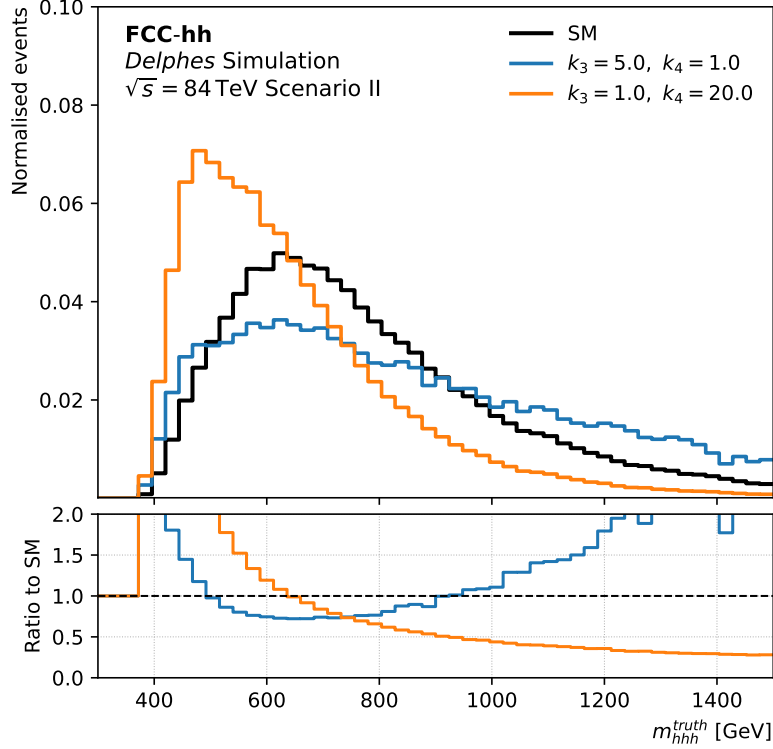


Fig. 7: Distributions of the truth HHH invariant mass, m_{HHH}^{truth} , for the SM prediction and two example (κ_3, κ_4) variations. No selection requirements are applied. Histograms are normalised to unit area, and the lower panel shows the ratio of the varied (κ_3, κ_4) models to the SM distribution.

the observed to the predicted value of the signal cross-section times branching ratio for that parameter point. Systematic uncertainties are included in the fit as nuisance parameters (NPs), denoted by the set $\vec{\theta}$, and are constrained by Gaussian or Poisson probability density functions. The 68% and 95% confidence level exclusions are obtained using the frequentist CLs prescription [26] with the profile likelihood ratio test statistic [27]:

$$\tilde{q}_\mu = -2 \log \left(\frac{\mathcal{L}(\mu, \hat{\theta}_\mu)}{\mathcal{L}(\hat{\mu}, \hat{\theta})} \right), \quad (4)$$

where the numerator indicates the value of θ that maximises \mathcal{L} for a given value of μ , and the denominator is evaluated for the values of $\hat{\mu}$ and $\hat{\theta}$ which jointly maximise the likelihood.

Four fits are performed using the **TRexFitter** framework [28]. Firstly, an upper-limit scan is performed for the SM HHH cross-section, with the limits corresponding to the 95% CL. Secondly, independent variations to (κ_3, κ_4) are considered across the plane using a 2D likelihood scan. Given that LHC measurements currently favour κ_3

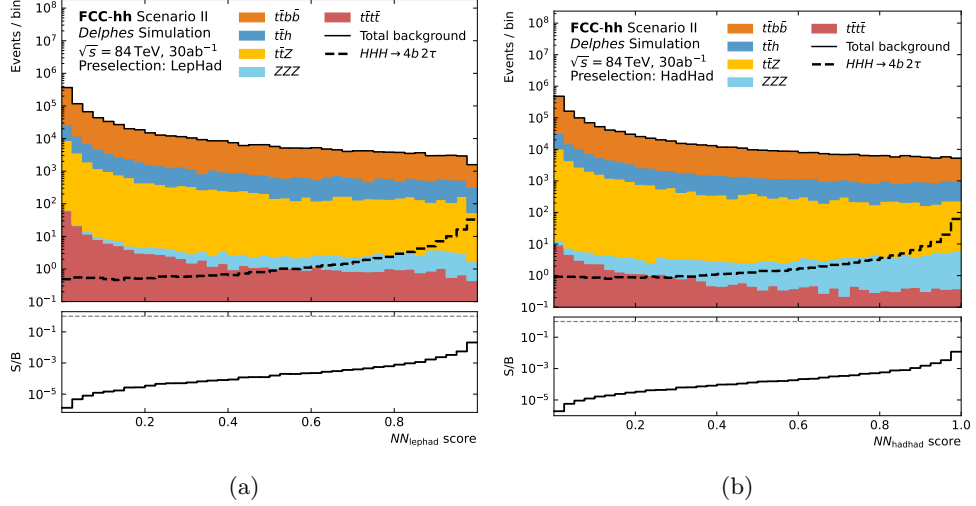


Fig. 8: Distribution of the (a) NN_{LePhad} and (b) NN_{hadHad} scores for the signal and background events. The lower panel shows the signal to background ratio in each bin.

values close to the SM prediction [29], a third fit is performed in which κ_3 is fixed to its SM value while κ_4 is varied, effectively probing the quartic coupling in isolation. Finally, a fit scanning κ_3 values for $\kappa_4 = 1$ is performed, to evaluate the sensitivity to κ_3 alone.

6 Systematic uncertainties

Systematic uncertainties are considered on the b -jet and τ -lepton identification efficiencies and the integrated luminosity determination. Two scenarios are defined for particular performance regimes as indications of the analysis' sensitivity to detector design; a case without systematic uncertainties 'No syst' is also evaluated to illustrate their impact. In Scenario I: b -jet and τ_{had} efficiency uncertainties are estimated to be 1% per-object, leading to total uncertainties of 4.1(2.0)% for b -jet (τ) identification respectively in $\text{SR-}\tau_{\text{lep}}\tau_{\text{had}}$ and $\text{SR-}\tau_{\text{had}}\tau_{\text{had}}$. Additionally, the luminosity uncertainty is taken to be a 1% variation in the expected yields in $\text{SR-}\tau_{\text{lep}}\tau_{\text{had}}$ and $\text{SR-}\tau_{\text{had}}\tau_{\text{had}}$. In Scenario II: b -jet and τ_{had} efficiency uncertainties are estimated to be 2% per-object, leading to overall 8.2 (4.0)% uncertainties for b -jet (τ) identification respectively in the in $\text{SR-}\tau_{\text{lep}}\tau_{\text{had}}$ and $\text{SR-}\tau_{\text{had}}\tau_{\text{had}}$. Additionally, the luminosity uncertainty is taken to be a 2% variation in the expected yields in $\text{SR-}\tau_{\text{lep}}\tau_{\text{had}}$ and $\text{SR-}\tau_{\text{had}}\tau_{\text{had}}$.³

³We note that both scenarios are extremely conservative, as background yields and experimental identification efficiencies are expected to be determined through data-derived approaches, significantly constraining experimental systematics and also reducing theoretical ones.

7 Results

The expected yields of signal and background samples are shown in Table 3. The signal yields remain small, illustrating the need for good control of background processes, and further work to optimise the selection efficiency.

Table 3: Expected nominal HHH signal and SM background yields in SR- $\tau_{\text{had}}\tau_{\text{had}}$ and SR- $\tau_{\text{lep}}\tau_{\text{had}}$.

	HHH	Total SM	$t\bar{t}$	$t\bar{t}H$	$t\bar{t}Z$	ZZZ	$t\bar{t}t\bar{t}$	S/\sqrt{B}
SR- $\tau_{\text{had}}\tau_{\text{had}}$	44	2210	1760	340	108	2.6	0.26	0.94
SR- $\tau_{\text{lep}}\tau_{\text{had}}$	19	390	310	63	15	0.44	0.09	0.95

The expected 95% CL upper limit on the SM cross-section upper limit of 10.5 fb, corresponding to $3.0 \times \sigma_{HHH}^{SM}$ at $\sqrt{s} = 84$ TeV. This is calculated using the Scenario I systematic uncertainty set-up. For comparison, the ATLAS Run-2 result [4] placed a limit of 59 fb, $760 \times \sigma_{HHH}^{SM}$ at $\sqrt{s} = 13$ TeV.

The expected simultaneous limits on the Higgs self-coupling modifiers κ_3 and κ_4 are shown in Figure 9, with the respective negative log-likelihood values shown in Figure 10. The systematic uncertainty Scenario I is used for the fit results. Comparisons across each systematic Scenario, at the 68% CL, are shown in Figure 11. As expected from the smallness of the signal and the systematic uncertainties’ conservatism, their impact is significant, motivating the use of data-derived approaches to constrain them.

Independent likelihood scans are performed for each coupling modifier, scanning over one κ value with the other fixed at the SM prediction of unity. The likelihood scan results are shown in Figure 12, with 68% and 95% CL levels indicated. The two systematic uncertainty Scenarios, and the ‘No syst’ scenario are shown. Assuming $\kappa_3 = 1$, κ_4 is restricted to be with the range $[-5.6, 21]$ $([-10, 25])$ at 68% (95%) CL, in the Scenario I systematic uncertainty setup. This situation would be indicated if SM HH is observed at HL-LHC or FCC-ee. Instead assuming $\kappa_4 = 1$, κ_3 is restricted to be with the range $[-0.44, 3.3]$ $([-1.0, 4.3])$ at 68% (95%) CL, in the Scenario I systematic uncertainty setup.

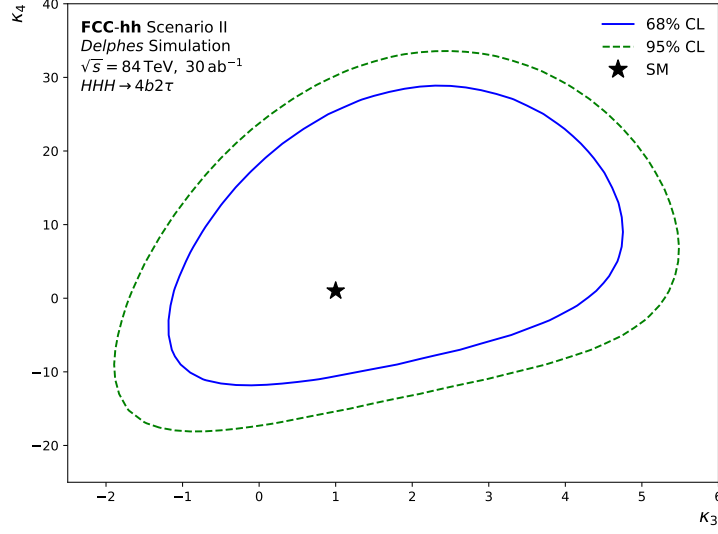


Fig. 9: Expected 95% and 68% CL constraints on κ_3 and κ_4 from the combined fit of the $\tau_{\text{lep}}\tau_{\text{had}}$ and $\tau_{\text{had}}\tau_{\text{had}}$ channels, in dashed and solid lines respectively. The SM prediction is indicated with the star at (1, 1). The systematic uncertainty Scenario I is used for the fit results.

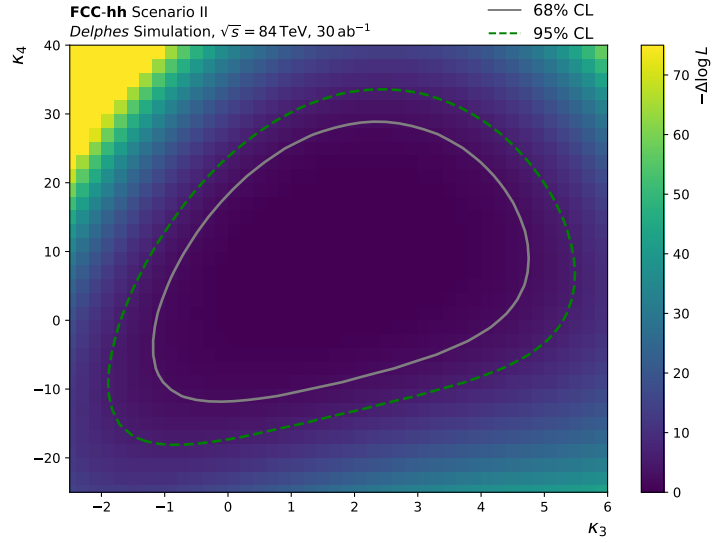


Fig. 10: Expected 95% and 68% CL constraints on κ_3 and κ_4 from the combined fit of the $\tau_{\text{lep}}\tau_{\text{had}}$ and $\tau_{\text{had}}\tau_{\text{had}}$ channels, in dashed and solid lines respectively. The negative log-likelihood values are shown in the coloured heat-map. The systematic uncertainty Scenario I is used for the fit results.

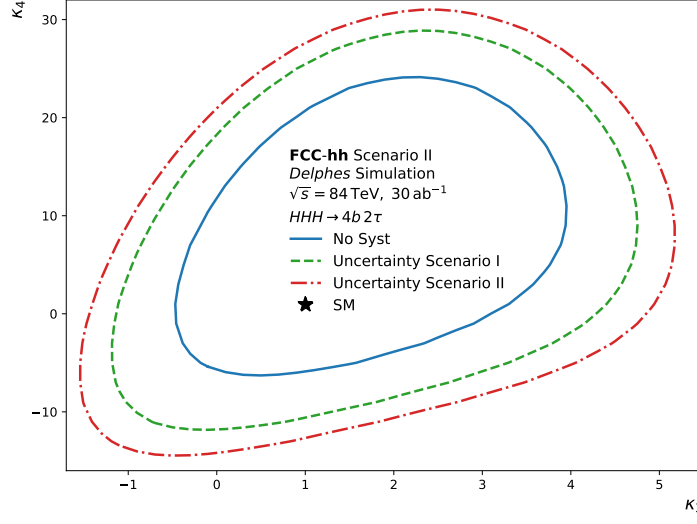
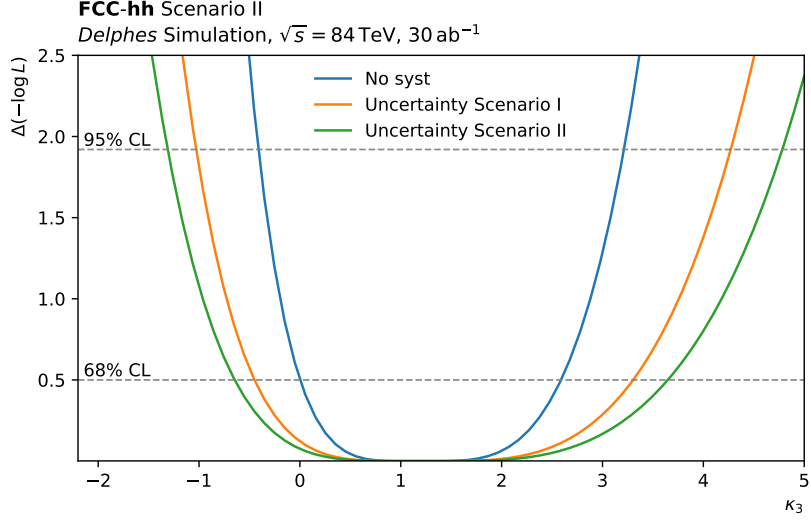
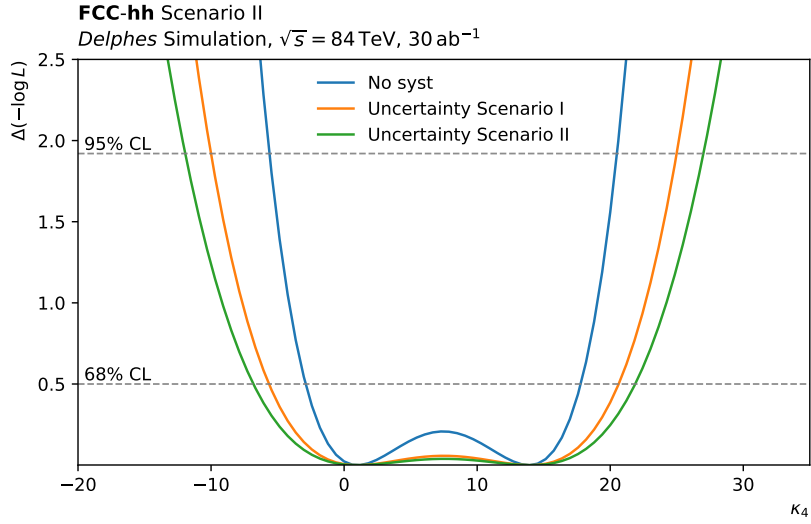


Fig. 11: Expected 68% CL constraints on κ_3 and κ_4 from the combined fit of the $\tau_{\text{lep}}\tau_{\text{had}}$ and $\tau_{\text{had}}\tau_{\text{had}}$ channels for the No Syst, Scenario I and Scenario II systematic scenarios are drawn in solid, dashed and dot-dashed lines respectively. The SM prediction is indicated with the star at (1,1).



(a)



(b)

Fig. 12: One-dimensional likelihood scans over the Higgs self-coupling modifiers (a) κ_3 and (b) κ_4 from the combined fit of the $\tau_{\text{lep}}\tau_{\text{had}}$ and $\tau_{\text{had}}\tau_{\text{had}}$ channels. Both of the modifiers are profiled in the profile-likelihood fit, and the likelihood scan of each parameter keeps the other fixed at one. The expected likelihood contour is shown, with the 68% and 95% CL horizontal lines are overlaid. The systematic uncertainty Scenario I is used for the fit results.

8 Conclusions

A key goal of the FCC-hh experimental programme is understanding the Higgs potential. A feasibility study of the potential of the tri-Higgs boson production at FCC-hh in the $4b2\tau$ final state has been performed, considering both $\tau_{\text{lep}}\tau_{\text{had}}$ and $\tau_{\text{had}}\tau_{\text{had}}$ channels and their combination. Considering an expected centre-of-mass energy, $\sqrt{s} = 84$ TeV, and a conservative jet flavour identification uncertainty, a 95% upper cross-section limit of $3 \times \sigma_{HHH}^{SM}$ is expected, with $\tau_{\text{had}}\tau_{\text{had}}$ providing the greater sensitivity. The sensitivity of this analysis to constrain the (κ_3, κ_4) parameter space is evaluated for several uncertainty scenarios. Percent level precision on κ_3 is anticipated through HH measurements, with this result constraining $-5.6 < \kappa_4 < 21$ at 68% CL for $\kappa_3 = 1$ in the baseline uncertainty Scenario I. Further improvements to this analysis may be possible from better optimised selections and jet tagging techniques, improved $m_{\tau\tau}$ and m_{bb} reconstruction and use of m_{HHH} information. Combinations with other channels of comparable sensitivity, such as $4b2\gamma$, will prove powerful and constitute a key FCC result.

Acknowledgements

This work has been partly supported by the Future Circular Collider Innovation Study (FCCIS) project, that has received funding from the European Union's Horizon 2020 research and innovation programme under grant No 951754. JF acknowledges support from the Royal Society (University Research Fellowship Renewals Grant URF/R/221037).

References

- [1] L.H.C.S.W. Group, A. David, A. Denner, M. Duehrssen, M. Grazzini, C. Grojean, G. Passarino, M. Schumacher, M. Spira, G. Weiglein, M. Zanetti. Lhc hxswg interim recommendations to explore the coupling structure of a higgs-like particle (2012). URL <https://arxiv.org/abs/1209.0040>
- [2] W. Bizoń, U. Haisch, L. Rottoli, Constraints on the quartic Higgs self-coupling from double-Higgs production at future hadron colliders. *JHEP* **10**, 267 (2019). [https://doi.org/10.1007/JHEP10\(2019\)267](https://doi.org/10.1007/JHEP10(2019)267). [arXiv:1810.04665](https://arxiv.org/abs/1810.04665) [hep-ph]
- [3] W. Bizoń, U. Haisch, L. Rottoli, Z. Gillis, B. Moser, P. Windischhofer, Addendum to: Constraints on the quartic Higgs self-coupling from double-Higgs production at future hadron colliders [JHEP 10 (2019) 267]. *JHEP* **02**, 170 (2024). [https://doi.org/10.1007/JHEP02\(2024\)170](https://doi.org/10.1007/JHEP02(2024)170). [arXiv:2402.03463](https://arxiv.org/abs/2402.03463) [hep-ph]
- [4] ATLAS Collaboration, Search for triple Higgs boson production in the $6b$ final state using pp collisions at $s=13$ TeV with the ATLAS detector. *Phys. Rev. D* **111**(3), 032006 (2025). <https://doi.org/10.1103/PhysRevD.111.032006>. [arXiv:2411.02040](https://arxiv.org/abs/2411.02040) [hep-ex]

- [5] CMS Collaboration, Search for triple Higgs production in Run 2 data of CMS using $4b2\gamma$ final state. CMS-PAS-HIG-24-015 (2025). URL <https://cds.cern.ch/record/2937680>
- [6] ATLAS Collaboration, HL-LHC prospects for the measurement of triple Higgs production in the $6b$ final state at the ATLAS experiment. ATL-PHYS-PUB-2025-003 (2025). URL <https://cds.cern.ch/record/2924772>
- [7] P. Stylianou, G. Weiglein, Constraints on the trilinear and quartic Higgs couplings from triple Higgs production at the LHC and beyond. Eur. Phys. J. C **84**(4), 366 (2024). <https://doi.org/10.1140/epjc/s10052-024-12722-9>. arXiv:2312.04646 [hep-ph]
- [8] D. de Florian, I. Fabre, J. Mazzitelli, Triple Higgs production at hadron colliders at NNLO in QCD. JHEP **03**, 155 (2020). [https://doi.org/10.1007/JHEP03\(2020\)155](https://doi.org/10.1007/JHEP03(2020)155). arXiv:1912.02760 [hep-ph]
- [9] D. de Florian, et al., Handbook of LHC Higgs Cross Sections: 4. Deciphering the Nature of the Higgs Sector (2017). <https://doi.org/10.23731/CYRM-2017-002>. arXiv:1610.07922 [hep-ph]
- [10] M.A. et. al., Conceptual design of an experiment at the fcc-hh, a future 100 tev hadron collider (2022). <https://doi.org/10.23731/CYRM-2022-002>
- [11] A. Abada, M. Abbrescia, S.e.a. Abdus-Salam, FCC-hh: The Hadron Collider. Eur. Phys. J. Spec. Top **228**, 755–1107 (2019). <https://doi.org/10.1140/epjst/e2019-900087-0>
- [12] M. Selvaggi, DELPHES 3: A modular framework for fast-simulation of generic collider experiments. J. Phys. Conf. Ser. **523**, 012033 (2014). <https://doi.org/10.1088/1742-6596/523/1/012033>
- [13] M. Selvaggi, B. Stapf, A delphes parameterisation of the fcc-hh detector (2025). <https://doi.org/10.17181/fgx1g-y0r44>
- [14] G. Ganis, C. Helsens, V. Völkl, Key4hep, a framework for future HEP experiments and its use in FCC. Eur. Phys. J. Plus **137**(1), 149 (2022). <https://doi.org/10.1140/epjp/s13360-021-02213-1>. arXiv:2111.09874 [hep-ex]
- [15] J. Alwall, M. Herquet, F. Maltoni, O. Mattelaer, T. Stelzer, MadGraph 5: going beyond. JHEP **06**, 128 (2011). [https://doi.org/10.1007/JHEP06\(2011\)128](https://doi.org/10.1007/JHEP06(2011)128). arXiv:1106.0522 [hep-ph]
- [16] C. Bierlich, S. Chakraborty, N. Desai, L. Gellersen, I. Helenius, P. Ilten, L. Lönnblad, S. Mrenna, S. Prestel, C.T. Preuss, T. Sjöstrand, P. Skands, M. Uthmeim, R. Verheyen, A comprehensive guide to the physics and usage of PYTHIA 8.3. SciPost Phys. Codeb. p. 8 (2022). <https://doi.org/10.21468/>

- [17] O. Mattelaer, On the maximal use of monte carlo samples: re-weighting events at nlo accuracy. The European Physical Journal C **76**(674) (2016). <https://doi.org/10.1140/epjc/s10052-016-4533-7>. URL <https://doi.org/10.1140/epjc/s10052-016-4533-7>
- [18] A. Papaefstathiou, K. Sakurai, Triple Higgs boson production at a 100 TeV proton-proton collider. JHEP **02**, 006 (2016). [https://doi.org/10.1007/JHEP02\(2016\)006](https://doi.org/10.1007/JHEP02(2016)006). arXiv:1508.06524 [hep-ph]
- [19] M. Cacciari, G.P. Salam, G. Soyez, The anti- k_t jet clustering algorithm. JHEP **04**, 063 (2008). <https://doi.org/10.1088/1126-6708/2008/04/063>. arXiv:0802.1189 [hep-ph]
- [20] A. Tumasyan, et al., Identification of hadronic tau lepton decays using a deep neural network. JINST **17**, P07023 (2022). <https://doi.org/10.1088/1748-0221/17/07/P07023>. arXiv:2201.08458 [hep-ex]
- [21] H. Qu, L. Gouskos, ParticleNet: Jet Tagging via Particle Clouds. Phys. Rev. D **101**(5), 056019 (2020). <https://doi.org/10.1103/PhysRevD.101.056019>. arXiv:1902.08570 [hep-ph]
- [22] A. Elagin, P. Murat, A. Pranko, A. Safonov, A New Mass Reconstruction Technique for Resonances Decaying to di-tau. Nucl. Instrum. Meth. A **654**, 481–489 (2011). <https://doi.org/10.1016/j.nima.2011.07.009>. arXiv:1012.4686 [hep-ex]
- [23] F. Pedregosa, G. Varoquaux, A. Gramfort, V. Michel, B. Thirion, O. Grisel, M. Blondel, P. Prettenhofer, R. Weiss, V. Dubourg, J. Vanderplas, A. Passos, D. Cournapeau, M. Brucher, M. Perrot, E. Duchesnay, Scikit-learn: Machine learning in Python. Journal of Machine Learning Research **12**, 2825–2830 (2011). URL <http://jmlr.org/papers/v12/pedregosa11a.html>
- [24] T. Akiba, S. Sano, T. Yanase, T. Ohta, M. Koyama. Optuna: A next-generation hyperparameter optimization framework (2019). URL <https://arxiv.org/abs/1907.10902>
- [25] M. Stone, Cross-validated choice and assessment of statistical predictions. J.Roy.Statist.Soc.B **36**(2), 111–147 (1974). <https://doi.org/10.1111/j.2517-6161.1974.tb00994.x>
- [26] A.L. Read, Presentation of search results: the CL_S technique. J. Phys. G **28**, 2693 (2002). <https://doi.org/10.1088/0954-3899/28/10/313>
- [27] G. Cowan, K. Cranmer, E. Gross, O. Vitells, Asymptotic formulae for likelihood-based tests of new physics. Eur. Phys. J. C **71**, 1554 (2011). <https://doi.org/10.1140/epjc/s10052-011-1554-0>. arXiv:1007.1727 [physics.data-an]

- [28] M. Aly, T. Dado, A. Held, M. Pinamonti, L. Valery, Trefitter (1.2.0). (2025).
<https://doi.org/10.5281/zenodo.15524537>
- [29] ATLAS Collaboration, Combination of Searches for Higgs Boson Pair Production in pp Collisions at $\sqrt{s}=13$ TeV with the ATLAS Detector. Phys. Rev. Lett. **133**(10), 101801 (2024). <https://doi.org/10.1103/PhysRevLett.133.101801>.
[arXiv:2406.09971](https://arxiv.org/abs/2406.09971) [hep-ex]